Abstract. Using new observations of the galaxy cluster AC 118 at intermediate redshift ($z = 0.31$) in the K_s band, we were able to detect the cluster from the center to half the Abell radius (1.5 Mpc, $H_0 = 50$ km s^{-1} Mpc^{-1}) and possibly to 2.0 Mpc. The analysis of both the spatial distribution of galaxies of various luminosities and of the luminosity function (LF) of galaxies in different cluster locations strongly confirms and extends to larger clustercentric radii the luminosity segregation found in a previous analysis of this cluster restricted to a smaller cluster area: there is an excess of bright galaxies in the cluster core (inside 250 Kpc) or a deficit of dwarfs in the remain part of the cluster. Outside the cluster core and as far as 1.5 or even 2 Mpc, the giant–to–dwarf ratio is constant. Because of the luminosity segregation, the LF of the AC 118 shows a larger number of bright galaxies per unit dwarf in the core than in other cluster locations. All non–core LFs, computed at several cluster locations, are compatible each other. These results hold both including or excluding the galaxies located in an overdensity found in the far South of AC 118 and in the second clump in galaxy density at the cluster North–West. Since the near–infrared emission is a good tracer of the stellar mass, we interpret the segregation found as a mass segregation.

Key words: Galaxies: evolution — Galaxies: clusters: general — Galaxies: clusters: individual: AC 118 = Abell 2744 — Galaxies: fundamental parameters — Galaxies: luminosity function, mass function — Galaxies: statistics

A&A manuscript no.
(will be inserted by hand later)

Your thesaurus codes are:
missing; you have not inserted them

K–band luminosity (mass) segregation in AC 118 at $z = 0.31^{\star}$

S. Andreon

INAF–Osservatorio Astronomico di Capodimonte, Via Moiariello 16, 80131 Napoli, Italy
E-mail: andreon@brera.mi.astro.it

Accepted 13 November 2001

1. Introduction

Field galaxies should experience interactions with the hostile cluster environment during infall in the cluster because of harassment (Moore et al. 1996), tidal tails and eventually mergers (Toomre & Toomre 1972) and possibly other cluster–specific phenomena. These effects influence infalling galaxies well before they reach the cluster core. Therefore, it is important to observe galaxies when interactions are occurring, i.e. at large clustercentric distances. The dependence of the galaxy properties on clustercentric distance is therefore informative of cluster–related phenomena.

Studies of galaxy evolution in clusters often sample only the cluster core because the cluster outskirts have a low contrast with respect to the background galaxies, making the measure of cluster galaxy properties subjected to large errors. Furthermore, the small field of view of the available imagers, in particular in the near–infrared, makes the sampling of the cluster outskirts expensive in telescope time. For these reasons, cluster outskirts are less frequently studied, in particular in the near–infrared, even if the near–infrared is very informative: for example it is a good tracer of the stellar mass (Bruzual & Charlot 1993; Pierini, Gavazzi & Boselli, 1996) and it is not too affected by short star bursts (Bruzual & Charlot 1993). Figure 10 in Andreon (2001) shows that there are only three investigations (de Propris et al. 1998; Andreon & Pelló 2000; Andreon 2001) sampling galaxies fainter than $M^* + 1$ and exploring radii larger than 0.4 Mpc. Since then, another work has appeared (Tustin, Geller, Kenyon & Diaferio 2001). The situation is now rapidly changing thanks to 2MASS (Skrutskie et al. 1997) and large panoramic infrared receivers, such as CIRSI (Mackay et al. 2000).

⋆ Based on observations collected at the European Southern Observatory, Chile, ESO N 62.O-0369, 63.O-0115, 64.O-0236

In this paper we make use of a large panoramic near–infrared receiver, an Hawaii chip, by imaging the intermediate redshift cluster AC 118. AC 118 has been observed with three pointings, two of which image the cluster outskirts and are presented in §2. The central pointing was, instead, presented in Andreon (2001, hereafter Paper I). In §3 the spatial distribution of galaxies of various luminosities, the dwarf to giant radial profile and the luminosity function at various cluster locations are presented. In §4 we present a summary and discuss the results.

In this paper we assume $H_0 = 50$ km s^{-1} Mpc^{-1} and $q_0 = 0.5$. The choice of the cosmology has a small or null impact on the results because all the compared galaxies are at the same redshift (see Sect 4).

2. Data and data reduction

AC 118, also known as Abell 2744 ($\alpha, \delta = 00\ 14\ 19.5\ -30\ 23\ 19,\ J2000$), is a cluster of galaxies at intermediate redshift ($z = 0.3$, see Paper I for a summary of its properties). Its central region has been imaged in the near–infrared K_s band with SOFI at NTT (Paper I). AC 118S and AC 118N, the northern and southern pointings of AC 118, have been observed in the K_s band in September 18 and October 31, 1999, respectively, with SOFI at NTT in the frame of an observational program aimed at deriving the Fundamental Plane at $z \sim 0.3$, as a complement to our central pointing. SOFI is equipped with a 1024×1024 pixel Rockwell "Hawaii" array, with a 0.292 arcsec pixel size and a 5×5 arcmin field of view. The two pointings are offset, with respect to the previous central pointing, by almost one SOFI field of view, to maximize the survey area while keeping enough overlap to check the consistency of the photometry of the three pointings (see Figure 1 for the pointing layout).

Table 1 gives a summary of the characteristics of the data used in this paper. Exposures times are shorter and observations are shallower, with respect to the central field, by a factor ~ 3 because of reduced time for near–infrared observations.

The data have been reduced as described in Paper I. Briefly, images are flat–fielded by means of differential dome flats and calibrated by means of Persson et al. (1998) standard stars. The background is removed by a temporal filtering of the images, using Eclipse (Devillard, 1997). The combining of the individual exposures is performed by means of *imcombine* under IRAF, making full use of the bad pixel mask and weights and aligning images without resampling. As in Paper I, the dependence of the atmospheric absorption on airmass is computed from the science data, since the target is observed at different hour angles.

Two (minor) differences apply with respect to the data reduction described in Paper I: a) the illumination correction is found to be significant, and applied to, AC 118S frames;

b) a residual shallow spatial gradient is present in the frames, even after the background subtraction performed via a filtering in the time domain. Therefore, we introduce a further step in the background subtraction, by fitting, and removing a plane to the background.

The two nights were photometric, as determined from the scatter of the zero point of the standard stars and from the scatter, from frame to frame, of the instrumental magnitudes of a reference galaxy in the field of view. For objects in common between fields, that are independently calibrated, we found systematic differences less than 0.01 mag, confirming the quality of the observing nights and of the data reduction.

During the September run (AC 118S), SOFI suffered a point spread function variable over the field, while in October the problem was largely solved.

Objects are detected and classified by SExtractor (Bertin & Arnouts 1996), version 2, using the exposure map for a clean detection.

Because of the shallower images, the 4.4 arcsec aperture (24 Kpc for cluster galaxies) adopted in Paper I is not an optimal aperture to measure the flux of our faint galaxies because the aperture integrates mainly noise (outer regions of faint galaxies are undetected) at a such a large radius. We adopt, therefore, a smaller (3.0 arcsec) aperture for the flux determination. By using the deep (central) AC 118 pointing we verify that such an aperture misses part of the galaxy flux, even for faint galaxies, i.e. the 3.0 arcsec aperture magnitude is not a surrogate for the "total" magnitude.

The sample is complete down to $K_s = 20$ mag in the most shallow field (AC 118S), and therefore the analysis is bound at $K_s \leq 20$ mag over the whole field of view.

3. Results

3.1. Spatial distribution of galaxies of various luminosities

Figure 1 shows the studied field of view. Each ellipse correspond to one galaxy[1]. The three dotted rectangles enclose the three K_s pointings. Attentive inspection of Figure 1 shows that:

– There are two obvious galaxy overdensities: one in the center and the other one at 3 arcmin NW.

– There is another possible overdensity in the far S, at ~ 5 arcmin away from the center, as can be appreciated by comparing the density of galaxies at similar distances from the cluster center in the Southern and Northern pointings. Galaxies in the far S have

[1] In the high density regions, the size and orientation of galaxies are determined with low accuracy because of crowding, but they are never used in this paper, except in this Figure for pictorial purposes.

unknown redshifts, and therefore we don't know whether this overdensity is associated with the cluster or is a background group (or cluster).

Figure 2 shows the cluster radial profile, i.e. the number of galaxies per radius bin, measured in circular annuli. It has been computed for four magnitude ranges and both including (open points) and excluding (close points) galaxies in the far S, that are possibly unrelated to the studied cluster, and in the NW quadrant, where the effect of the NW clump should be higher. The radial profiles are statistically background subtracted in order to remove interlopers by using the background galaxy density measured in the HDF-S (da Costa et al. 2002), as computed by ourselves by using their public images. Errors are assumed to be Poissonian (i.e. for the time being we neglect the intrinsic variance of galaxy counts, that are, instead, taken into account in the next sections). The area observed at each radius is shown in Figure 3, and care should be paid to densities computed over a small area (say, much less than 2 arcmin^2) and large clustercentric radii because on these small areas the intrinsic variance of the galaxy counts could be very large with respect to the low cluster galaxy density.

The cluster radial profile of all galaxies (brighter than $K_s < 20$ mag, or $M_K \lesssim -21$ mag, upper–left panel) shows a positive galaxy density from the center to 2 Mpc away, in particular when galaxies in the far S are counted. It is centrally peaked. When the NW quadrant is included in the profile computation, a second broad peak is present at 0.7 Mpc from the cluster center, while at larger radii the profile decreases. When the quadrant including the NW clump is instead removed, the radial profile shows a flattening, instead of a second maximum, at ~ 1 Mpc from the cluster center.

When we consider only galaxies brighter than $K_s = 17$ mag ($M_K \sim -24$ mag), i.e. massive galaxies, the cluster radial profile (upper–right panel) is steeper in the center than in the previous case, because the galaxy density increases by a factor 7 over three bins, to be compared to an increase of a factor 2 to 3 over the same radial range when all galaxies are considered. The second maximum is still there when all galaxies are counted (open points). Overall, the profile is quite flat outside the cluster core. The evidence of a positive density at 1.8 Mpc is marginal (2σ) when discarding galaxies in the far S, while it is significant including them.

At the other end of the luminosity function, the radial profile of faint galaxies, $19 < K_s < 20$ mag or $-22 \lesssim M_K \lesssim -21$ mag, is quite flat from the center to $\sim 1 - 1.2$ Mpc (bottom–right panel), and undetected (i.e. statistical evidence is $\sim 1\sigma$) at large radii, even binning the data with larger bins.

The shape of spatial distributions of galaxies in the $18 < K_s < 20$ mag (bottom–left panel) and $19 < K_s < 20$ (bottom–righ panel) ranges are quite similar. There is a factor of two between the amplitudes of the two radial profiles, because there is a factor of

two between the two considered magnitude ranges, and because the AC 118 luminosity function is quite flat at these magnitudes (see Section 3.3). The innermost point seems higher that the ones at $r \sim 1$ arcmin, but without any statistical significance.

Therefore, the radial profile of all, bright and faint galaxies are quite different in steepness. Faint galaxies shows similar radial profiles independent of the two considered magnitude ranges.

3.2. Dwarfs to giant ratio radial profile

The left panel of figure 4 shows the giant–to–dwarf ratio, as a function of the clustercentric distance. For the sake of clarity, galaxies brighter than $K_s = 17$ ($M_K \sim -24$) mag are called giants, while galaxies with $18 < K_s < 20$ mag are called dwarfs. The giant–to–dwarf ratio shows a maximum at the center, where there are similar numbers of giant and dwarfs in the considered magnitude range, then decreases to a much smaller value from radii as small as 300 Kpc and as far as 2.2 Mpc. Outside the cluster core, there are roughly 3 dwarfs per giant in the considered magnitude ranges. The deficit of dwarfs in the cluster core (or the excess of giants) is in agreement with that found in the previous Figure and in Paper I by analysing the shape of the LF at various cluster locations (but over a restricted cluster portion) and of the giant–to–dwarf ratio at a few cluster locations. The inclusion or exclusion of the NW quadrant or of the far S region does not appreciably change the giant–to–dwarf ratio, as shown in the Figure. The new data presented in this paper do not make stronger the statistical significance of the found segregation for clustercentric distance less than 1 Mpc (that it is claimed significant at > 99.9 % confidence level in Andreon 2001), because new data are at larger clustercentric distances. Since we divide the $R < 1$ Mpc range in three bins, instead of the two bins as in Paper I, the statistical evidence *per bin* is in fact smaller here than in Paper I ($>\sim 90$ vs > 99.9 % confidence level). At the large clustercentric radii sampled by the new data, the giant–to–dwarf ratio differs from the central one at the 90 % confidence level when all the field of view is considered, and at the 80 % confidence level when the NW quadrant and the far S regions are excluded. In this specific calculation, we take into account the field–to–field background variance as described in Huang et al. (1997), and we propagate the errors as described in Gehrels (1986), i.e. we do not make the simplifying assumption of Gaussian errors.

Similar conclusions can be drawn defining as dwarfs $19 < K_s < 20$ mag galaxies (right panel of Figure 4), except that the absolute value of the giant–to–dwarf ratio increases by approximatively a factor of two, because the considered magnitude range for dwarfs is now half the size. The shapes of the giant–to–dwarf radial profiles in the two panel of Figure 4 are striking similar. This similarity implies that $19 < K_s < 20$ mag dwarfs are

not segregated with respect to $18 < K_s < 20$ mag dwarfs, as directly seen in the bottom panels of Figure 2.

Note, however, that the smaller magnitude range adopted in the right panel of Figure 4 also decreases the number of dwarfs, and therefore increases the size of error bars. For the same reason the statistical significance of a variation of the giant–to–dwarf ratio is also reduced.

3.3. Luminosity function at various cluster locations

The LF is computed as the statistical difference between (crowding–corrected) galaxy counts in the cluster direction and in the control field direction. We use the HDF-S (da Costa et al. 2002) as background (control) field, and we fully take into account the field–to–field galaxy count fluctuations in the error computation (see Paper I for details).

We fitted a spline to the background counts and we use it in place of the observed data points because background galaxy counts show an outlier point at $K_s = 17$ mag when a 3 arcsec aperture is adopted.

The present AC 118 sample consists of 496 members, about as many galaxies as in Paper I, but are distributed over a larger area and a narrower magnitude range. The LF has been fitted by a Schechter (1976) function by taking into account the finite bin width (details are given in Paper I). Figure 5 shows the LF computed at different cluster locations and the best fit Schechter (1976) function to the global (i.e. those measured over the whole field of view) LF, whose ϕ^* is scaled by the ratio between the number of members at each location and in the global LF. The global LF is shown in panel a). Panels b) and c) present the LF of the main and secondary clumps, respectively. Their exact boundary definitions are those of Paper I (for a pictorial view see Fig. 1 there). Panel d) shows the LF of galaxies inside the central pointing but outside the two clumps. Panels e) shows the LF of galaxies in the Northern and Southern pointings (not overlapping with the central pointing) and not in the far S. Finally, panel f) shows the LF of the galaxies in the far S (southest 1 arcmin).

The best fit parameters to the global LF are: $K_s^* = 16.4$ mag ($M_{K_s^*} \sim -24.9$ mag) and $\alpha = -0.85$, where α is the slope of the faint part of the LF, and M^* is the knee of the LF, i.e. the magnitude at which the LF starts to decrease exponentially. We re–state that the present 3 arcsec magnitude misses a significant part of the galaxy flux, and hence the found parameters should not be used for, say, computing the luminosity density, or for comparison with values derived from other samples using a different metric (or any isophotal) aperture. This could also be appreciated by noting that in Paper I, using magnitudes that include a large fraction of the galaxy flux, we found steeper LFs than shown in panel b), c) and d) for the same considered cluster and background regions. Here

we use the LF as a tool for comparing the abundance of galaxies of various luminosities in different environments for a sample of galaxies all at the same redshift and whose flux is measured in one single way. A thorough discussion of the cosmological implication of lost flux from galaxies is given in Wright (2001) and Andreon (2002). Errors, quoting the projection of the $\Delta\chi^2 = 2.3$ (68% for two interesting parameters, Avni 1976) confidence contours on the axis of measure are: 0.35 mag and 0.21, respectively, for K_s^* and α. The conditional errors, i.e. the errors when the other parameters are kept at the best values (that has a low statistical sense, Press et al. 1992) are found to be at least half the size[2] . The AC 118 global LF is smooth and is well described by a Schechter function ($\chi^2/\nu \sim 4.2/8$).

The parameters of the global LF also describe the shape of the LF measured at other cluster locations (see panels from *c*) to *f*)), because the reduced χ^2 is of the order of 1 or less, except for the LF in panel *b*). Galaxies considered in panel *b*) are in the cluster center: for the total number of observed galaxies there are a too many very bright galaxies (say, brighter than $K_s = 16 - 17$ mag) and too few fainter galaxies, an effect already found in Paper I for the same region and using the same data, but adopting a magnitude definition which includes a larger galaxy flux. This is the same effect shown in Figures 2 and 4 and presented in the previous sections, measured here by looking for differences in the LF computed at several cluster locations instead of looking for a dependence between the spatial distribution of galaxies and their luminosities. Differences found in Paper I are confirmed here (by adopting a ~ 95 % confidence level threshold and using a Kolmogorov–Smirnov test, that is preferable to comparing the best fit values because of the correlation between parameters and of the need for an assumption of a given parental distribution): the LF is flatter at the main clump (panel *b*)) than at all the other considered regions. All the other LFs are compatible each other at better than 95% confidence level, extending at larger radii the findings in Paper I: the LF steepens going from high– to low– density environments and the steepening stops in the region considered in panel *d*). The new result is that the LF does not change in regions not surveyed in Paper I, i.e. for galaxies whose average clustercentric projected distance is 1.2 Mpc (for galaxies in the N and S pointings, panel *e*)) and 1.8 Mpc (for galaxies in the far S, panel *f*).

The *f*) panel only includes galaxies in the far S (southest 1 arcmin). These galaxies are an extension of the AC 118 cluster, or another group (or part of a cluster) along the line of sight. Given the small number of galaxies in this region (56 galaxies out of 535) and the similarity of their LF to the global one, their inclusion or exclusion from the global LF makes no difference.

[2] and are often quoted in the literature (forgetting the adjective "conditional").

The LFs computed thus far can be used to test whether the galaxy overdensity in the far S is at the AC 118 redshift, under the assumption that the LF is a standard candle outside the cluster core. The use of the near–infrared LF as a standard candle has been exploited by de Propris et al. (1999) to study the luminosity evolution of galaxies up to $z \sim 1$. There are two paths for the computation, depending on whether a parametric form is used for the LF shape (and in such a case the errors on the data points are included in the confidence level calculation) or no (that neglects errors on data points). For galaxies in the far S sample, the 68 % conditional confidence range (i.e. once α is keep fix to the best fit value) for M^* are 16.3 and 17.9 mag, limiting the difference in distance modulus between AC 118 and the far S overdensity to $\Delta(m-M) = -0.1, +1.5$ mag or, in redshift, -0.01,+0.3. This range in $\Delta(m-M)$ only excludes that the galaxies in the far S are in the AC 118 foreground. To be precise, the high redshift constraint is broader, because our 3 arcsec aperture includes more and more galaxy flux as the redshift increases, and we have not accounted for this effect. By using the data points alone and a Kolmogorov–Smirnov test, the 68 % confidence range is $\Delta(m-M) = 0, \sim 1.7$ mag, quite similar to the parametric result. Therefore, the analysis of the LF is not sufficient to say whether these galaxies belong to the cluster of are in the background of AC 118. Surely, these galaxies do not lie in front of the cluster.

In conclusion, the analysis of the luminosity function shows the same luminosity segregation found in the analysis of the galaxy spatial distribution. With respect to Paper I, we extended the analysis to much larger distances (1.8 Mpc vs 0.58 Mpc).

4. Summary and discussion

We detect AC 118 from the center to half the Abell radius (1.5 Mpc) and possibly to 2.0 Mpc.

There is a luminosity segregation among the galaxies in the AC 118 cluster and it has been shown in three different ways: by studying the LF dependence on environment, by a radial analysis of the dwarf–to–giant ratio and by comparing the radial profiles of galaxies of different luminosities. While the three methods differ, they are not independent. It is the order in which the grouping is done that changes: galaxies are first grouped spatially and then their luminosity distribution is studied in the LF analysis, while in the two other methods galaxies are first grouped in luminosity and then their spatial distribution is studied.

Any choice of cosmology rigidly moves the upper abscissa of Figure 2, 3, 4 and 5 by a fixed amount, and does not change the shape or relative differences of the plotted profiles. Therefore, the detection of a luminosity segregation in AC 118 is independent of the choice of the cosmological values.

The segregation concerns mainly the inner 250 Kpc of the cluster (see in particular Figure 4), while at larger radii all galaxies have the same spatial distribution regardless of the galaxy near–infrared luminosity, up to 2 Mpc away from the cluster center. The segregation consists of an excess, of a factor of 3, of giants galaxies in the cluster core (or in a deficit, of the same factor, of dwarf galaxies). Since the numerical density of dwarfs is largely constant, the luminosity segregation found seems due to an excess (relative to the number of dwarf galaxies) of giant galaxies in the cluster center, and not due to a deficit of dwarfs in the remaining of the cluster.

Beside AC 118, luminosity segregation in the near–infrared has been suggested in the Coma cluster (Andreon & Pelló 2000), although through comparison of heterogeneous data.

The luminosity segregation found in Paper I is here confirmed to hold over a even wider cluster region. With respect to the previous investigation on AC 118, we take two more paths for confirming the luminosity segregations: the analysis of the galaxy spatial distribution, and the computation of the radial profile of the giant to dwarf ratio. Our results are in broad agreement with what has been found in similar analyses, but performed at optical wavelengths (Zwicky 1957, Mellier et al. 1988; Driver, Couch & Phillipps 1998; Secker, Harris & Plummer 1997; Garilli, Maccagni & Andreon 1999), or by using the velocity segregation (Chincarini & Rood 1977; Struble 1979; Biviano et al. 1992; Stein 1997), or by analysing the galaxy angular correlation function (Loveday et al. 1995): these studies found that brightest galaxies are more tightly correlated (or have lower velocity dispersions) than the faintest galaxies.

Therefore, there is clear evidence of luminosity segregation. Since the near–infrared luminosity is a good tracer of the stellar mass (Bruzual & Charlot 1993), the segregation found is interpreted a mass–related segregation. The luminosity segregation we found in the near–infrared implies a mass segregation more tightly that under the usual assumption than optical luminosity traces mass: here we show directly that massive galaxies are found preferentially in the cluster center.

A mass–related segregation is a natural expected outcome of a hierarchical scenario of cluster formation, because the clustering strength depends on the halo circular velocity (and therefore on mass) in cold dark matter models (White et al. 1987, Kauffmann et al. 1997). However, the effect has been detected only recently in the simulations (Springer, White, Tormen & Kauffman 2001) and a quantitative comparison between observations and simulations awaits a prediction in a more suitable form.

The hostile cluster environment plays a role in shaping the AC 118 LF but only at small clustercentric radii (or high density), since outside the cluster core the LF computed

at several locations are all compatible with each other and the dwarf–to–giant ratio is constant within the errors.

Acknowledgements. This work is part of a collaboration with M. Arnaboldi, G. Busarello, M. Capaccioli, G. Longo, P. Merluzzi and G. Theureau. A. Wolter and A. Iovino are acknowledged for useful discussions. The near–infrared observations presented in this paper have been taken during the NTT guaranteed time of Osservatorio di Capodimonte. The director of my institute, Prof. M. Capaccioli, is warmly thanked for permitting me a long stay at the Osservatorio Astronomico di Brera, where this work has been prepared. The director of the latter institute, Prof. G. Chincarini, is acknowledged for hospitality. Comments from the referee helped to improve the presentation of this paper.

References

Andreon S., 2001, ApJ, 547, 623 (Paper I)

Andreon S., 2002, A&A, in press

Andreon, S. & Pelló, R. 2000, A&A, 353, 479

Avni Y., 1976, ApJ 210, 642

Bertin E., & Arnouts S. 1996, A&AS, 117, 393

Biviano, A., Girardi, M., Giuricin, G., Mardirossian, F., & Mezzetti, M. 1992, ApJ, 396, 35

Bruzual A., G. & Charlot, S. 1993, ApJ, 405, 538

Chincarini, G. & Rood, H. J. 1977, ApJ, 214, 351

Da Costa L., Nonino M., Rengelink R., Zaggia S., Benoist C. et al., 2002, A&A, submitted (astro-ph/9812105)

de Propris, R., Stanford, S. A., Eisenhardt, P. R., Dickinson, M., & Elston, R. 1999, AJ, 118, 719

Devillard N., 1997, The Messenger 87, 19

Driver S. P., Couch W. J., Phillipps S 1998, MNRAS 301, 369

Garilli B., Maccagni D., Andreon S., 1999, A&A, 342, 408

Gavazzi, G., Pierini, D., & Boselli, A. 1996, A&A, 312, 397

Gehrels N., 1986, ApJ 303, 336

Huang J.-S., Cowie L. L., Gardner J. P., Hu E. M., Songaila A. & Wainscoat R. J., 1997, ApJ 476, 12

Kashikawa, N., Sekiguchi, M., Doi, M., Komiyama, Y., Okamura, S., Shimasaku, K., Yagi, M., & Yasuda, N. 1998, ApJ, 500, 750

Loveday, J., Maddox, S. J., Efstathiou, G., & Peterson, B. A. 1995, ApJ, 442, 457

Mackay, C. D. et al. 2000, Proc. SPIE, 4008, 1317

Mellier, Y., Mathez, G., Mazure, A., Chauvineau, B., & Proust, D. 1988, A&A 199, 67

Moore, B., Katz, N., Lake, G., Dressler, A., & Oemler, A. 1996, Nature, 379, 613

Persson S. E., Murphy D. C., Krzeminski W., Roth M., Rieke M. J. 1998, AJ 116, 2475

Schechter, P. 1976, ApJ, 203, 297

Secker, J., Harris, W. E. & Plummer, J. D. 1997, PASP, 109, 1377

Springel, V., White S., Tormen G., Kauffmann G., 2001, MNRAS, submitted (astro-ph/0012055)

Stein, P. 1997, A&A, 317, 670

Struble, M. F. 1979, AJ, 84, 27

Skrutskie, M., et al. 1997, in The Impact of Large Scale Near-IR Sky Surveys, ed. F. Garzon et al. (Dordrecht: Kluwer), 25

Toomre, A. & Toomre, J. 1972, ApJ, 178, 623

Tustin, A. W., Geller, M. J., Kenyon, S. J., & Diaferio, A. 2001, AJ, 122, 1289

White, S. D. M., Davis, M., Efstathiou, G., & Frenk, C. S. 1987, Nature, 330, 451

Wright, E. L. 2001, ApJ, 556, L17

Zwicky, F. 1957, Morphological astronomy, Berlin: Springer

Table 1. The data

	AC 118C	AC 118S	AC 118N
Exposure time (min)	265	75	90.7
Seeing (FWHM, arcsec)	0.75	1.0	1.2
Fully corrected noise[a] (mag arcsec^{-2})	24.0	23.0	23.3
Applied Illumination correction?	no	yes	no
Photom. zero–point RMS over the field (mag)	0.007	0.013	0.004

[a] The sky noise is measured as the dispersion of adjacent pixels in the background, once the image is binned in pixels of 1 arcsec.

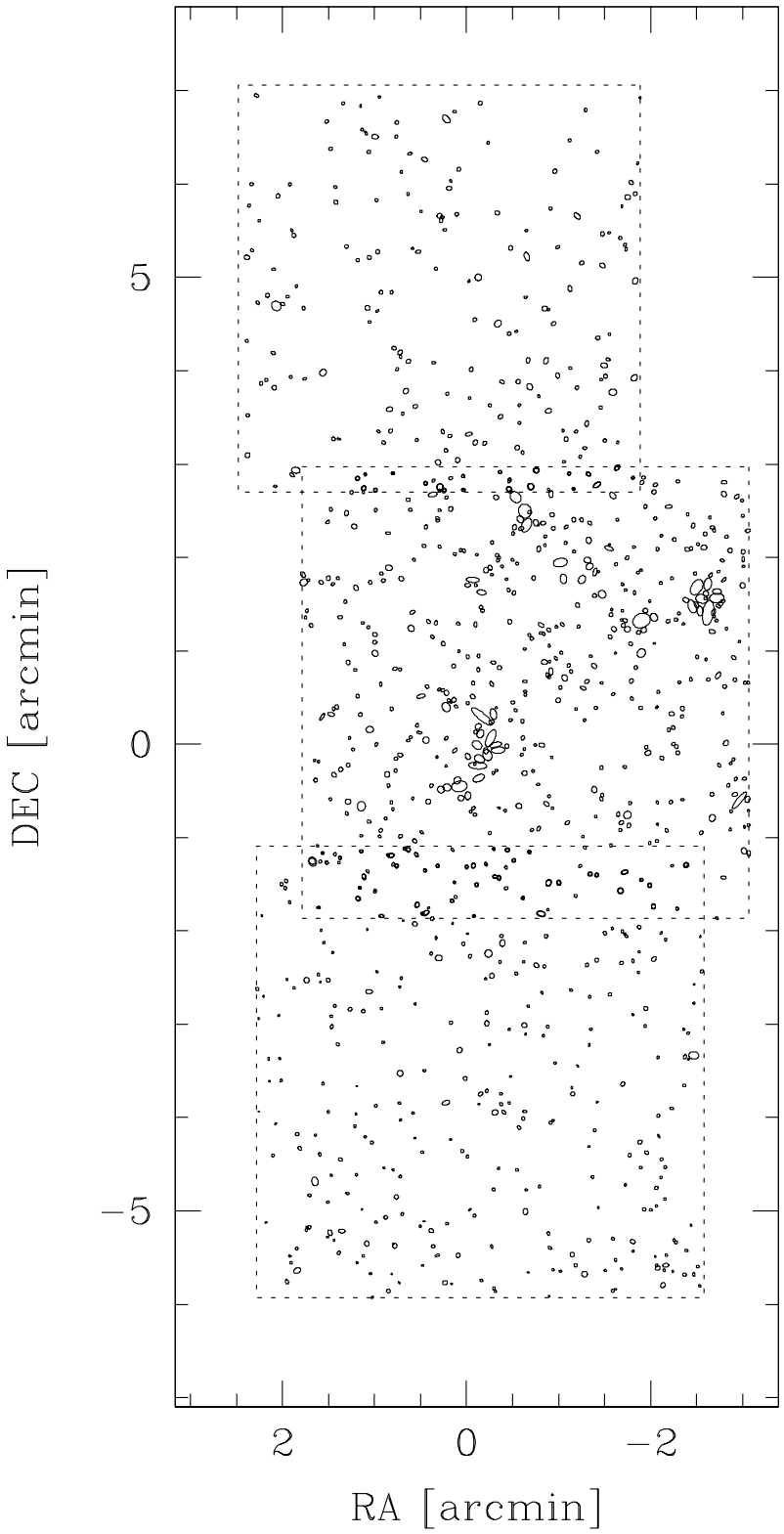

Fig. 1. Detected galaxies (ellipses), brighter than $K_s = 20$ mag, and X–ray contours. The area of ellipses is twice the galaxy isophotal area computed at 1.5σ above the background (20.8-21.8 mag arcsec^{-2}). North is up and East is to the left. The origin is at $(\alpha, \delta) = (00\ 14\ 20,\ -30\ 24\ 00)$ (J2000)

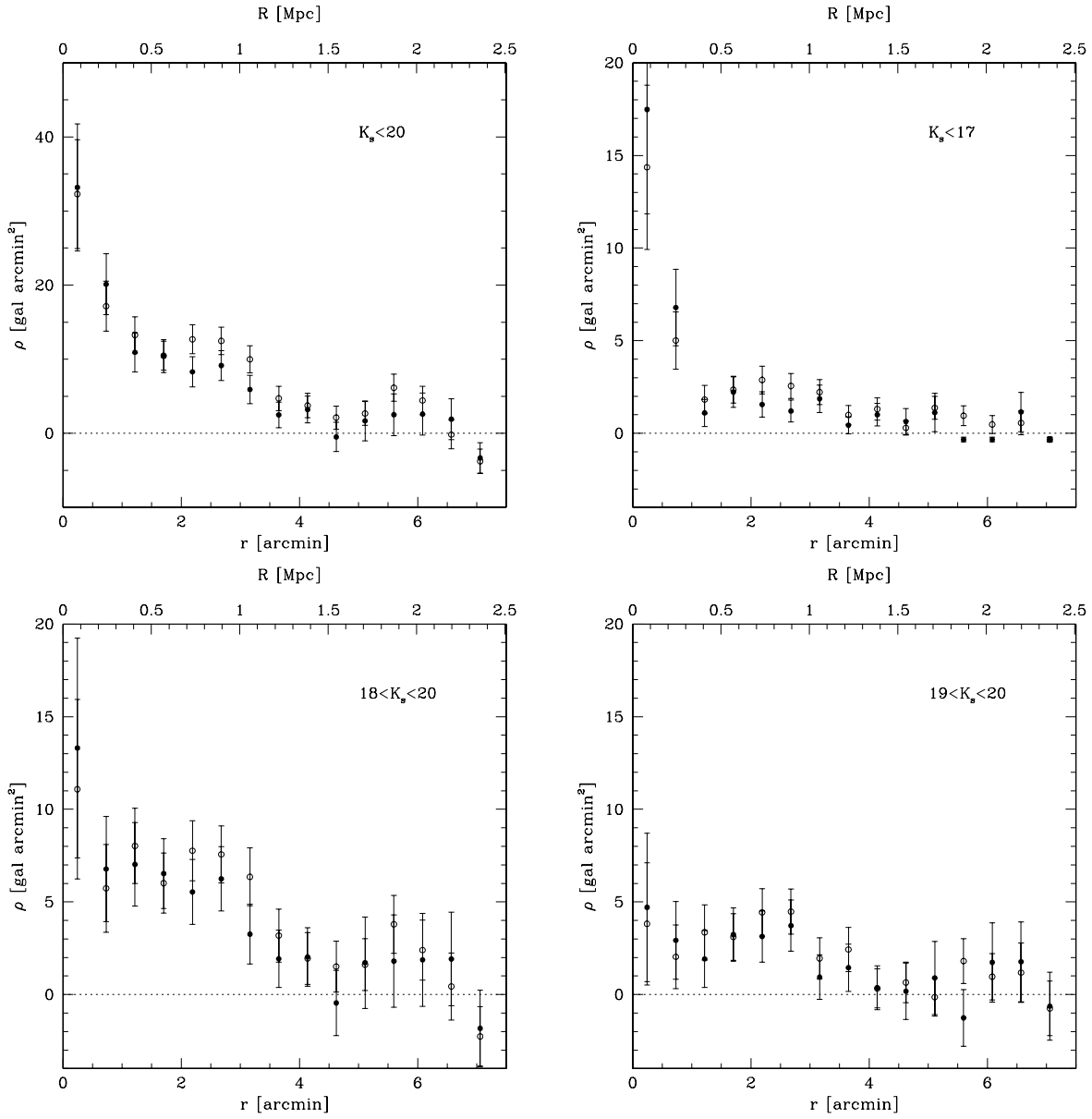

Fig. 2. Background subtracted radial profiles of the AC 118 cluster. Galaxies having $K_s < 20$, $K_s < 17$, $18 < K_s < 20$ and $19 < K_s < 20$ mag are selected for the computation of the radial profiles in the top–left, top-right, bottom–left and bottom–righ panels, respectively. Open dots show the profile computed over all the observed field, while closed points show the profile computed excluding the southest 1 armin and the NW quadrant. Note the steepness of the radial profile of bright galaxies (upper–right panel) and the flatness of the radial distribution of faint galaxies (lower–left panel). The density of background galaxies measured in the HDF-S is 7.8, 0.3, 6.3, 4.2 gal arcmin^{-2} for $K_s < 20$, $K_s < 17$, $18 < K_s < 20$ and $19 < K_s < 20$ mag respectively, when adopting our 3 arcsec aperture magnitude, and has been already subtracted.

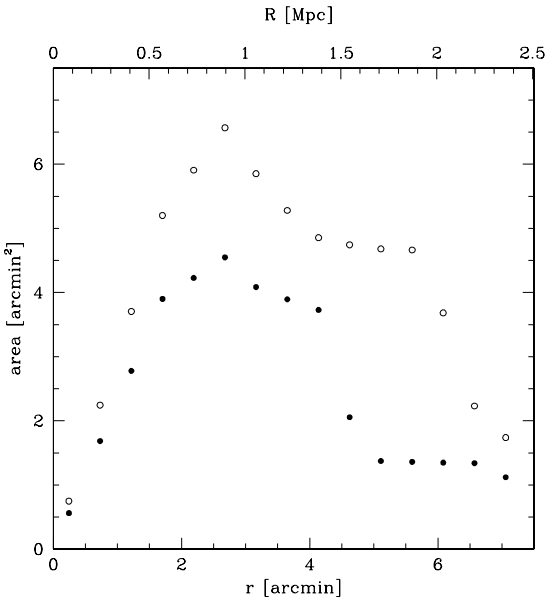

Fig. 3. Area over which the radial profiles are computed. Open points mark the area studied when all the field of view is considered, while close points mark the area when the NW quadrant and the southest 1 armin are excised.

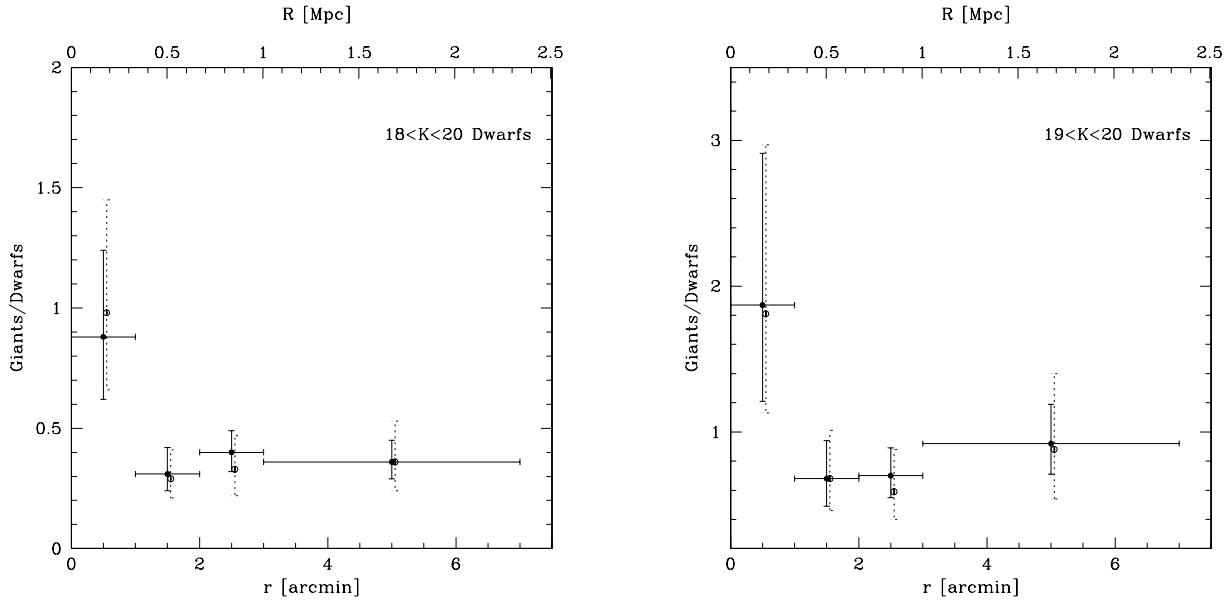

Fig. 4. Giant ($K_s < 17$) to dwarf ($18 < K_s < 20$ in the left panel, $19 < K_s < 20$ in the right panel) ratio as a function of the clustercentric distance, including and excluding the NW quadrant and the southest 1 armin (open and solid points, respectively). Error bars in the abscissa show the bin width. For display purposes error bars in the abscissa are drawn once and points are slightly displaced in x.

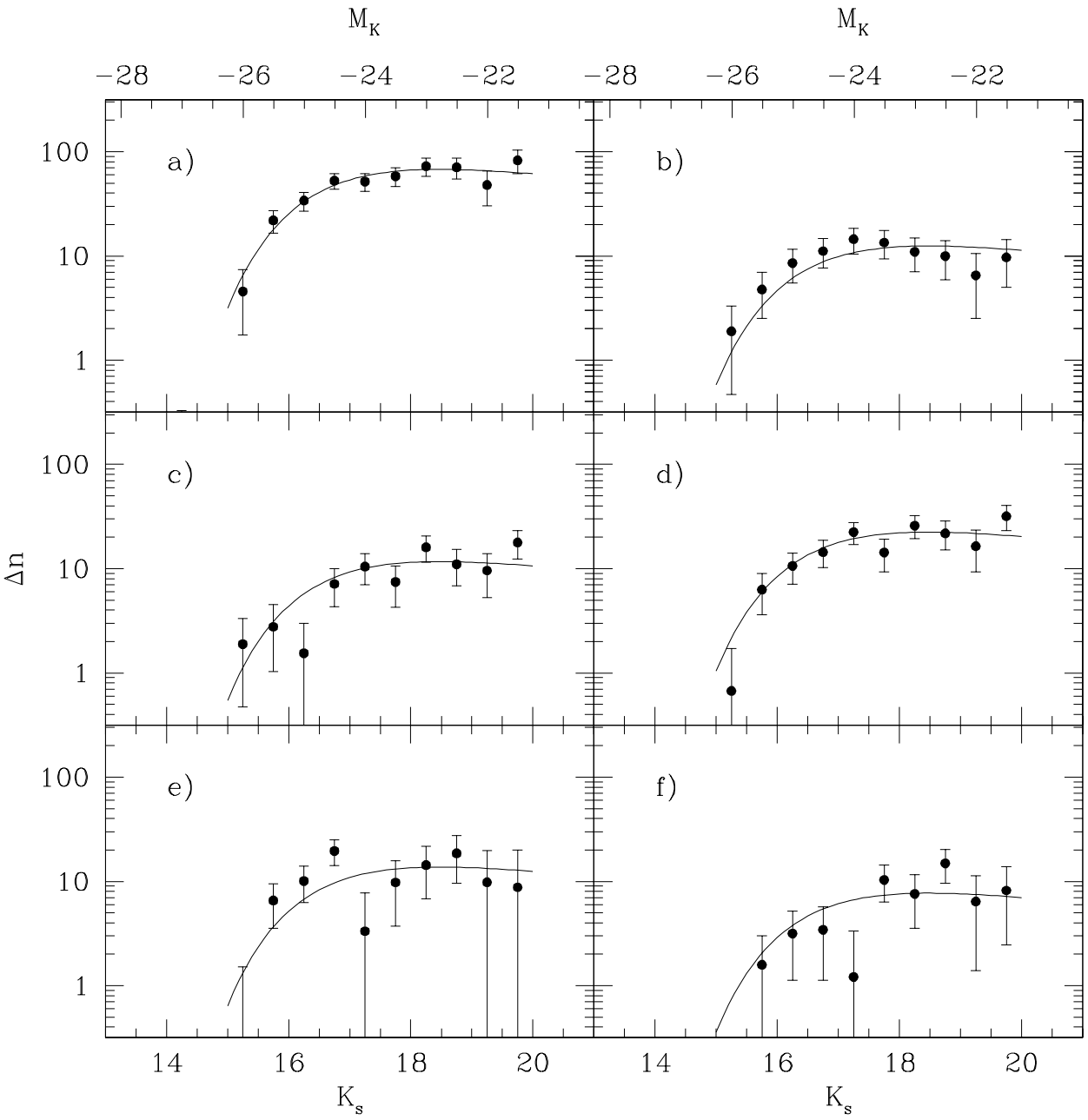

Fig. 5. Luminosity function of AC 118. The global (i.e. integrated over the whole studied field) LF is shown in panel *a*). Panels *b*) and *c*) present the LF of the main and secondary clumps, respectively. Panel *d*) is the LF of galaxies inside the central pointing but outside the two clumps. Panels *e*) shows the LF of galaxies in the Northern and Southern pointings (not overlapping to the central pointing) and not in the far S. Finally, panel *f*) shows the LF of the galaxies in the far S (southern 1 arcmin). The curve is the best fit function to the whole cluster, with ϕ^* adjusted to reproduce the total number of galaxies at each considered location. There are 496, 91, 86, 164, 101, 56 galaxies in panel a), b), c), d) e) and f), respectively.